

# Urea-Induced Drying of Hydrophobic Nanotubes: Comparison of Different Urea Models


Peng Xiu,<sup>†</sup> Zaixing Yang,<sup>†</sup> Bo Zhou,<sup>‡,§</sup> Payel Das,<sup>||</sup> Haiping Fang,<sup>‡</sup> and Ruhong Zhou<sup>\*,||</sup>

<sup>†</sup>Bio-X Lab, Department of Physics, Zhejiang University, Hangzhou 310027, China

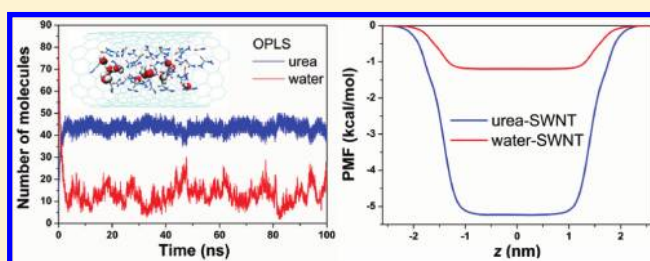
<sup>‡</sup>Shanghai Institute of Applied Physics, Chinese Academy of Sciences, P.O. Box 800-204, Shanghai 201800, China

<sup>§</sup>Graduate School of the Chinese Academy of Sciences, Beijing 100080, China

<sup>||</sup>Computational Biology Center, IBM Thomas J. Watson Research Center, 1101 Kitchawan Road, Yorktown Heights, New York 10598, United States

 Supporting Information

**ABSTRACT:** In a previous study, we performed the molecular dynamics (MD) simulations of various carbon nanotubes solvated in 8 M urea and observed a striking phenomenon of urea-induced drying of hydrophobic nanotubes, which resulted from the stronger dispersion interaction of urea than water with nanotube (Das, P.; Zhou, R. H. *J. Phys. Chem. B* 2010, 114, 5427–5430). In this paper, we have compared five different urea models to investigate if the above phenomenon is sensitive to the urea models used. We demonstrate through MD simulations that the drying phenomenon and its physical mechanism are qualitatively independent of the urea models. Consistent with our previous study, our current analyses with both interaction potential energy and association free energy indicate that there is a “dry state” inside the carbon nanotubes, which is caused by the urea’s preferential binding to nanotubes through stronger dispersion interactions. These results also have implications for understanding the urea-induced protein denaturation by providing further evidence of the potential existence of a “dry globule”-like transient state during protein unfolding and the “direct interaction mechanism” (whereby urea attacks protein directly, rather than disrupts water structure as a “water breaker”). In addition, our study highlights the crucial role of dispersion interaction in the selective absorption of molecules in hydrophobic nanopores and may have significance for nanoscience and nanotechnology.



## 1. INTRODUCTION

Urea is a widely used protein denaturant.<sup>1</sup> Despite extensive studies,<sup>2–19</sup> the molecular picture of urea-induced denaturation of proteins is still a subject of considerable debate, particularly the dominant driving force and the intermediates involved in the process. Two different mechanisms have been proposed to understand the urea-induced denaturation: an “indirect mechanism”, which comprises two aspects: urea denatures protein either through disrupting the structure of water, thus making hydrophobic groups more readily solvated,<sup>2–6</sup> or through modifying the lifetime or strength of the hydrogen bond between water and protein;<sup>7–10</sup> and a “direct mechanism” in which urea is presumed to affect the protein structure via direct electrostatic/van der Waals (vdW) interactions with protein.<sup>11–20</sup> It should be noted that protein denaturing via both the direct and indirect mechanisms has been emphasized by some literature as well.<sup>6,8–10,21,22</sup>

Recently, Stumpe and Grubmüller<sup>17</sup> performed molecular dynamics (MD) simulations of chymotrypsin inhibitor 2 (CI2) in 8 M urea and found the urea-induced protein unfolding proceeded primarily not by active attack but by a favorable interaction of urea with transiently exposed, less-polar residues and the protein backbone, thereby impeding the hydrophobic

collapse of partially unfolded proteins toward the native state. However, another MD simulation<sup>6</sup> of CI2 in 8 M urea showed that the first step in unfolding was expansion of the hydrophobic core, which was solvated by water and later by urea. Similarly, Wei et al.<sup>8</sup> also found water penetrated into the hydrophobic cores of protein HP-35 and its mutant ahead of urea, thus inducing the expansion of hydrophobic cores, which were then further solvated and stabilized through interactions with both water and urea, especially urea. They proposed that urea changed the activity of water, thus facilitating the penetration of water into the hydrophobic cores of proteins. In combination with their previous work,<sup>23</sup> they postulated that this indirect effect of urea was especially important when the hydrophobic space was too small for urea to penetrate into. In contrast, Hua et al.<sup>19</sup> found that urea-induced denaturation of proteins was dominantly driven by stronger dispersion interaction of urea with protein than water, and urea penetrated the hydrophobic core before water, forming a “dry globule”, followed by global unfolding of

**Received:** September 1, 2010

**Revised:** December 24, 2010

**Published:** March 08, 2011

**Table 1.** Nonbonded Parameters for OPLS, KBFF, CHARMM, AMBER\*, and AMBER Urea Models (See Text for the Detailed Descriptions of These Urea Models)<sup>a</sup>

model		O	C	N	H
OPLS	<i>q</i>	−0.390	0.142	−0.542	0.333
	$\sigma$	0.296	0.375	0.325	0.000
	$\epsilon$	0.878 64	0.439 32	0.711 28	0.000 00
KBFF	<i>q</i>	−0.675	0.921	−0.693	0.285
	$\sigma$	0.310	0.377	0.311	0.158
	$\epsilon$	0.560	0.417	0.500	0.088
CHARMM	<i>q</i>	−0.510	0.510	−0.620	0.310
	$\sigma$	0.302 91	0.356 36	0.329 63	0.040 00
	$\epsilon$	0.502 08	0.460 24	0.836 80	0.192 46
AMBER*	<i>q</i>	−0.613 359	0.880 229	−0.923 545	0.395 055
	$\sigma$	0.295 99	0.339 97	0.325 00	0.106 91
	$\epsilon$	0.878 64	0.359 82	0.711 28	0.065 69
AMBER	<i>q</i>	−0.495	0.933	−0.925	0.353
	$\sigma$	0.295 99	0.339 97	0.325 00	0.106 91
	$\epsilon$	0.878 64	0.359 82	0.711 28	0.065 69

<sup>a</sup> The units of *q*,  $\sigma$ , and  $\epsilon$  are *e*, nm, and kJ/mol, respectively.

the protein. Unfortunately, the transient nature of the proposed dry globule and the complicated structure of the hydrophobic core of protein make the further investigations very difficult. In a previous study,<sup>24</sup> by using MD simulations, we have designed some model systems with the single-walled carbon nanotubes (SWNTs) to investigate the urea-induced denaturation of proteins and found a striking phenomenon of urea-induced drying of the hydrophobic nanotubes. However, in that study, only the CHARMM urea model<sup>25</sup> was used, and it was unclear if the conclusions will be sensitive to different force fields or more specifically different urea models. There are some other urea models, such as OPLS,<sup>26,27</sup> KBFF<sup>28</sup> (force field derived from Kirkwood–Buff theory), and AMBER\*<sup>29</sup> urea models. The charge distributions of these urea models are quite different (see Table 1), which result in different electrostatic interactions. Consequently, the simulation results may differ from one another with different urea models.

In this paper, we use five different urea models (see “Model and Methods” for details) to study the dependence of the phenomenon of urea-induced drying of hydrophobic nanotubes on the urea models. Similar to our previous study, we also use the SWNT as the prototype of the hydrophobic core of protein, because the SWNT has a similar hydrophobic environment<sup>23</sup> and a comparable size (a few nanometers) to a protein interior.<sup>30</sup> Therefore, even though the chemical structure of a carbon nanotube is not exactly the same as a protein interior, the simulation results from our model system would still be helpful to understand the mechanism of urea-induced denaturation of proteins. In all of the five cases, we observe the drying phenomenon for both the wide nanotube [(17, 8) SWNT] and the narrow nanotube [(6, 6) SWNT]. This strikingly drying phenomenon is attributed to the stronger dispersion interaction of urea than water with nanotube. These results are consistent with our previous study.<sup>24</sup> Thus we conclude that the phenomenon of urea-induced drying of the hydrophobic nanotubes, together with its physical mechanism, are qualitatively independent of the urea models. We also compare the drying effects with different urea models. The present study implies the existence of a dry globule-like transient state during the urea-induced denaturation

of proteins and supports the “direct interaction mechanism” whereby urea has a stronger dispersion interaction with protein than water.<sup>19</sup> In addition, our study highlights the crucial role of dispersion interaction in the selective absorption<sup>31,32</sup> of molecules in hydrophobic nanopore.

## 2. MODEL AND METHODS

To study the influence of urea models on the phenomenon of urea-induced drying of the hydrophobic nanotubes, we have used five different urea models: OPLS,<sup>26,27</sup> KBFF,<sup>28</sup> CHARMM (parameters derived from the CHARMM22 force field<sup>25</sup>), AMBER\*,<sup>29</sup> and AMBER [parameters derived from the file embedded in the AMBER 10 simulation package (University of California at San Francisco)]. The OPLS and KBFF models are probably the most popular urea models,<sup>7,8,15–18,20,23,33–37</sup> and there are some previous studies on the comparison of these two models.<sup>15,34–37</sup> The CHARMM urea model is also widely used to study the process and mechanism of urea-induced denaturation of proteins.<sup>9,14,19,22,38</sup> The AMBER\* urea model has been used to study the urea-mediated dewetting between hydrophobic plates.<sup>21</sup> The molecular structures of the five urea models are slightly different (the molecular structures of OPLS and KBFF urea are identical, but they are slightly different from other models). However, the nonbonded parameters, especially the charge distributions, of these models are quite different (see Table 1 for the nonbonded parameters of the five urea models). Note that the OPLS and KBFF urea models use geometric combination rules for parameters of the Lennard-Jones 6–12 potential, whereas the CHARMM, AMBER\*, and AMBER urea models use Lorentz–Bertelot combination rules.

We have prepared two systems to study the phenomenon of urea-induced drying of SWNTs. The first one, namely, the (17, 8) SWNT system, contains a (17, 8) SWNT with dimensions of 3.155 nm in length and 1.729 nm in diameter, solvated in 8 M aqueous urea consisting of 747 urea and 3253 TIP3P<sup>39</sup> water molecules (see Figure 1A). Since the edge of the (17, 8) SWNT is irregular, only the axially central region of SWNT (2.555 nm in length) is considered when counting water/urea molecules for comparison. The second one, namely, the (6, 6) SWNT system, contains a (6, 6) SWNT with dimensions of 1.35 nm in length and 0.812 nm in diameter, solvated in 8 M aqueous urea consisting of 225 urea and 973 TIP3P water molecules (see Figure 3A). The (17, 8) and (6, 6) SWNTs were aligned along the *z*-axis in a cubic solvation box with initial side lengths of 5.55 and 3.75 nm, respectively.

The initial coordinates of SWNTs were generated using the nanotube builder plugin of VMD software.<sup>40</sup> The carbon atoms of SWNTs were modeled as uncharged Lennard-Jones particles with a cross-section of  $\sigma_{cc} = 0.34$  nm and a depth of the potential well of  $\epsilon_{cc} = 0.3598$  kJ mol<sup>−1</sup>.<sup>41,42</sup> The positions of the carbon atoms at the inlet and outlet were constrained by using the position restraint. Other carbon atoms were left free to vibrate. Carbon–carbon bond lengths and bond angles were maintained by harmonic potentials with spring constants of 392 460 kJ mol<sup>−1</sup> nm<sup>−2</sup> and 527 kJ mol<sup>−1</sup> rad<sup>−2</sup>. In addition, a weak dihedral angle potential was applied to bonded carbon atoms.<sup>41,42</sup>

All MD simulations were performed using Gromacs 4.0.7<sup>43</sup> in an NPT (300 K, 1 atm) ensemble. The constant temperature and pressure were maintained using a v-rescale thermostat<sup>44</sup> (with a coupling coefficient of  $\tau_T = 0.5$  ps) and Parrinello–Rahman pressure coupling scheme<sup>45</sup> (with a coupling coefficient of  $\tau_p = 5$  ps),

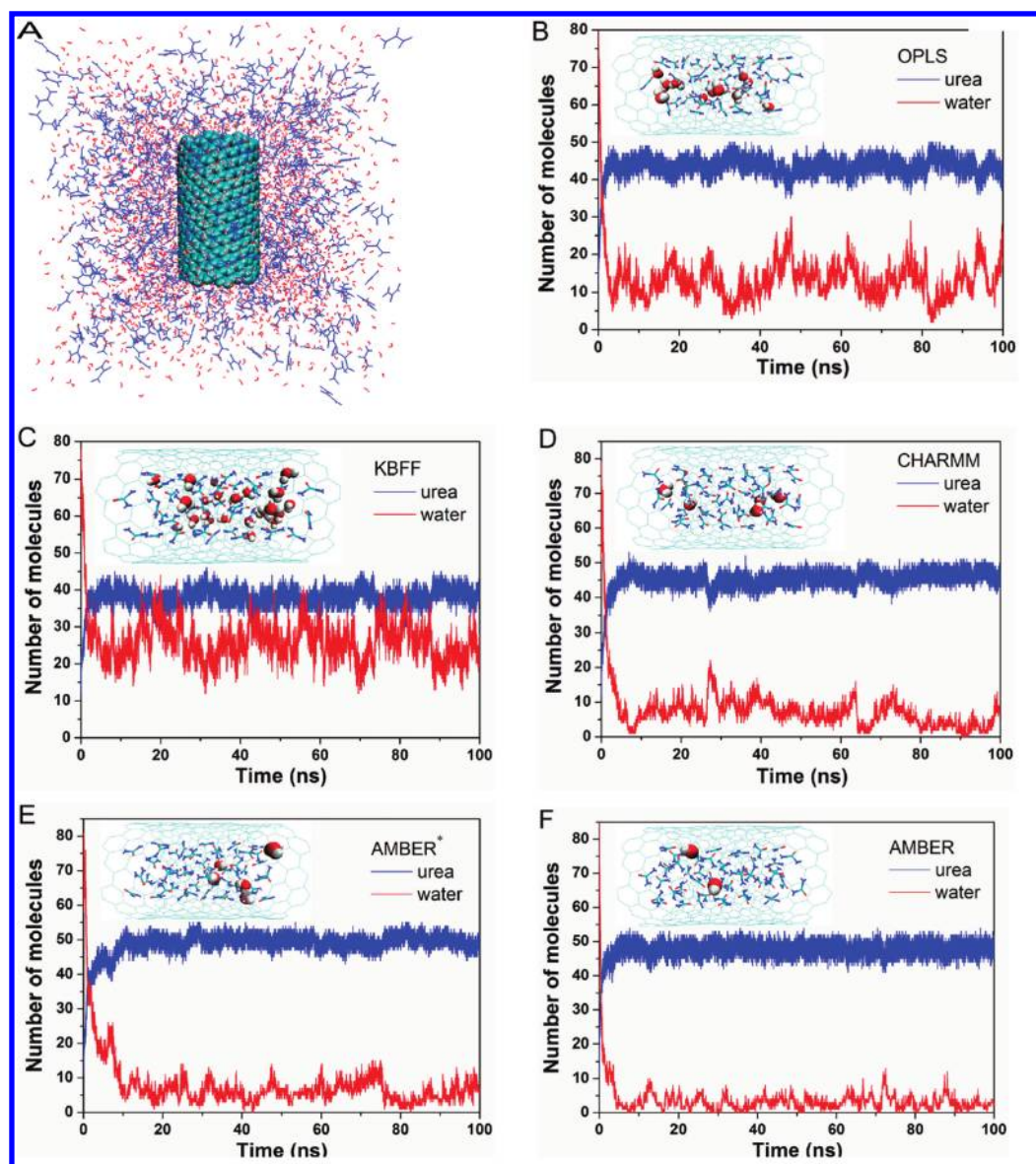


**Figure 1.** (A) Solvated system of (17, 8) single-walled carbon nanotube (SWNT) in 8 M aqueous urea (the SWNT is represented by vdW balls, and solvent, by wires with urea colored blue). (B–F) Number of urea (shown in blue) and water (shown in red) molecules within (17, 8) SWNT as a function of simulation time, with OPLS, KBFF, CHARMM, AMBER\*, and AMBER urea models, respectively. Inset: Corresponding structures of the urea–water mixture within (17, 8) SWNT in equilibrium (from an axial view), with urea represented by wires and water by vdW balls.

respectively. Periodic boundary conditions were applied in all directions. The particle-mesh Ewald method<sup>46</sup> with a real space cutoff of 1 nm was used to treat long-range electrostatic interactions, whereas the vdW interactions were treated with a cutoff distance of 1.2 nm. Lincs was applied to constrain all bonds. A time step of 2.0 fs was used, and data were collected every 1 ps. The simulation lengths for all systems were 100 ns.

### 3. RESULTS AND DISCUSSION

**3.1. Urea-Induced Drying for the (17, 8) SWNT System.** As a first quick comparison of different urea models, we have calculated the average urea dipole moments in bulk for the five urea models under ambient conditions (300 K, 1 atm). To calculate these dipole moments, we have performed five simulations of 616 urea molecules in a cubic box using different urea models.

Each simulation length was 10 ns, with the last 9 ns collected for analysis. The dipole moment for each urea model was averaged over all of the urea molecules in the cubic box. We note that for rigid urea models this is not needed in theory, but for flexible models this method of calculation takes into account the influence of thermal fluctuations under ambient conditions on the dipole moment of urea. The resulting dipole moments are 4.77, 4.65, 4.40, 4.65, and 3.19 D, for OPLS, KBFF, CHARMM, AMBER\*, and AMBER urea, respectively. These values for OPLS and KBFF urea are in good agreement with previous literature (4.9<sup>26</sup> and 4.65 D<sup>28</sup> for OPLS and KBFF urea, respectively), where the calculations of the dipole moment were based on a single urea molecule with an equilibrium geometry. For comparison, the experimental dipole moment of urea has been estimated to be 3.83 D<sup>47</sup> in the gas phase, 4.56 D<sup>48</sup> in dioxane, 4.2 D<sup>49</sup> in pure water, and 4.66 D<sup>50</sup> in the solid state. It is interesting to note



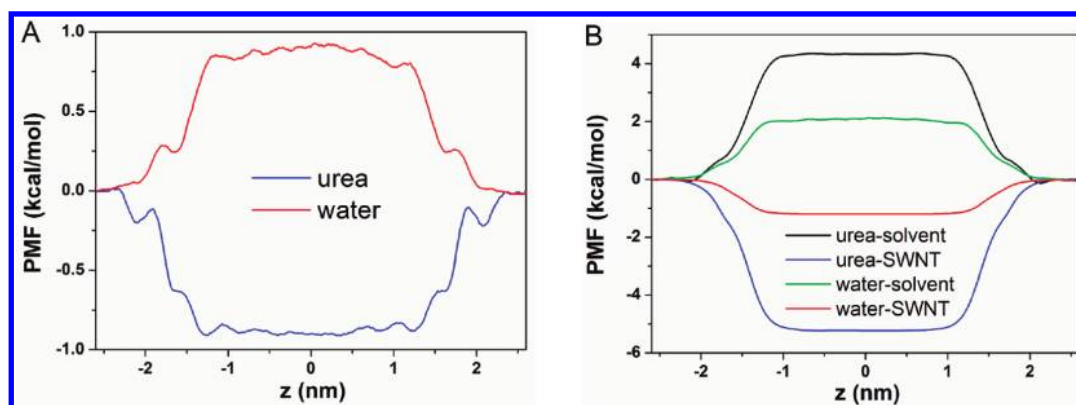


**Figure 2.** Association free energy of a solvent molecule with SWNT using the OPLS urea model for illustration. The calculated PMF profiles of a urea and a water molecule along the axis of the (17, 8) SWNT (located at  $-1.58 \text{ nm} \leq z \leq +1.58 \text{ nm}$  region). (A) Total PMF profiles. (B) Decomposition of total PMF profiles into solvent–solvent and solvent–SWNT interaction components.

**Table 2.** Average Number of Urea ( $\langle N_{\text{urea}} \rangle$ ) and Water Molecules ( $\langle N_{\text{water}} \rangle$ ) in (17, 8) SWNT, as Well as the Drying Factors,  $f_{\text{drying}}$  (See Text for Details), for Different Urea Models<sup>a</sup>

model	$\langle N_{\text{urea}} \rangle$	$\langle N_{\text{water}} \rangle$	$f_{\text{drying}}$
OPLS	43.6	12.8	14.8
KBFF	37.9	25.7	6.40
CHARMM	45.5	6.6	29.9
AMBER*	49.6	5.9	36.8
AMBER	47.8	2.9	71.7

<sup>a</sup> These data were averaged over the last 90 ns, wherein the systems have reached equilibrium.

that for OPLS, KBFF, CHARMM, and AMBER\* urea, although their charge distributions are quite different, their dipole moments are very similar (the dipole moments for KBFF and AMBER\* urea are almost identical). On the other hand, even though the two urea models can have identical dipole moments (for KBFF and AMBER\* urea), their behaviors in SWNT could be quite different (see below).

Parts B–F of Figure 1 show the number of solvent (water/urea) molecules inside the cores of (17, 8) SWNTs in 8 M aqueous urea during the course of MD simulation, for all five urea models. Here we define a solvent molecule to be inside the SWNT if the center of mass (COM) of it enters the SWNT. The corresponding snapshots of the urea–water mixture inside the nanotubes, after the systems have reached equilibrium, are also shown in the insets from an axial view. Surprisingly, in all five cases, most of the water molecules originally inside the SWNT (the urea concentration inside the SWNT is also roughly 8 M from the initial solvation setup) are expelled from the SWNT, and the hydrophobic cores are dominantly occupied by the urea molecules eventually. Table 2 lists the average number of urea ( $\langle N_{\text{urea}} \rangle$ ) and water molecules ( $\langle N_{\text{water}} \rangle$ ) in (17, 8) SWNTs with different urea models. These numbers are averaged over the time period wherein the systems have reached equilibrium ( $t \geq 10 \text{ ns}$ ). To quantify the drying effect and facilitate direct comparison among the results obtained with different urea models, we have calculated the “drying factor”  $f_{\text{drying}}$  defined as follows:

$$f_{\text{drying}} = R_{\text{SWNT}}/R_{\text{bulk}} \quad (1)$$

**Table 3.** Differences in Average Interaction Energies (kcal/mol) of a Solvent (Urea/Water) Molecule in (17, 8) SWNT vs in Bulk, with Different Urea Models<sup>a</sup>

model	$\Delta E_{\text{total}}^{\text{u}}$	$\Delta E_{\text{elec}}^{\text{u}}$	$\Delta E_{\text{vdW}}^{\text{u}}$	$\Delta E_{\text{total}}^{\text{w}}$	$\Delta E_{\text{elec}}^{\text{w}}$	$\Delta E_{\text{vdW}}^{\text{w}}$
OPLS	−2.57	3.91	−6.48	0.76	2.59	−1.83
KBFF	−2.55	3.32	−5.87	0.41	2.01	−1.60
CHARMM	−4.10	2.93	−7.03	0.71	2.53	−1.82
AMBER*	−4.58	2.17	−6.75	0.12	1.85	−1.73
AMBER	−4.32	2.60	−6.92	1.64	3.92	−2.28

<sup>a</sup>  $\Delta E_{\text{total}}^{\text{u}}$ ,  $\Delta E_{\text{elec}}^{\text{u}}$ ,  $\Delta E_{\text{vdW}}^{\text{u}}$  denote the differences in total, electrostatic, and vdW interaction energies, respectively, where  $\text{u}$  is u for urea and w for water. These data were averaged over the first 10 ns.

where  $R_{\text{SWNT}}$  and  $R_{\text{bulk}}$  are the ratio of the average number of urea to water molecules in SWNT, and that in the bulk region, respectively. A larger drying factor means a stronger drying effect induced by urea.  $f_{\text{drying}}$  for the (17, 8) SWNT system with different urea models are also shown in Table 2. From strong to weak, the drying effects for the five urea models are rank-ordered as AMBER, AMBER\*, CHARMM, OPLS, and KBFF. The drying effects for AMBER, AMBER\*, and CHARMM urea are so strong that almost all of the water molecules initially inside the nanotubes are expelled from the nanotubes after the systems have reached equilibrium. Even for the KBFF urea, whose drying effect is the weakest among the five urea models, it can expel most of the water molecules from the SWNT. These results strongly suggest that a dry globule-like state can be formed inside the SWNT, which also imply that urea might be able to penetrate a protein hydrophobic core ahead of water, forming some dry globule-like intermediates during the early stages of protein denaturation.

To explain the observed urea-induced drying of SWNTs from an energetic perspective, we computed the interaction energies of a solvent molecule in bulk (defined as 1.2 nm away from any atoms of SWNT for any atoms of the solvent) and in (17, 8) SWNT, with the rest of the system [see Tables S1 and S2 in the Supporting Information]. Table 3 lists the differences in average interaction energies for a solvent molecule in (17, 8) SWNT and in bulk, for all five urea models. As the solvent molecules move from the bulk region to the (17, 8) SWNT core, both urea and water molecules lose electrostatic interaction energies, but each urea gains more vdW interaction energy than water (about 3–4

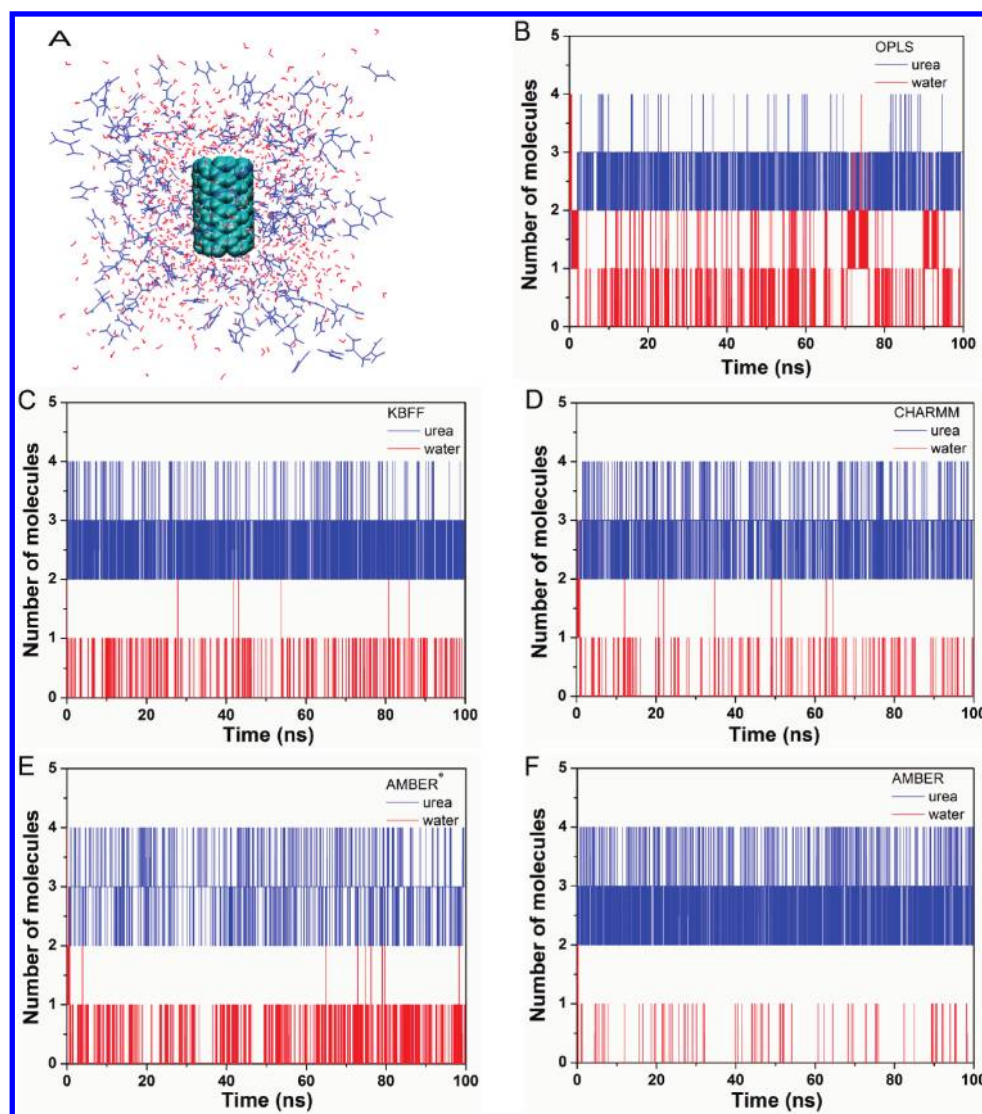


**Figure 3.** (A) Solvated system of (6, 6) SWNT in 8 M aqueous urea (the SWNT is represented by vdW balls, and solvent, by wires with urea colored blue). (B–F) Number of urea (shown in blue) and water (shown in red) molecules within (6, 6) SWNTs as a function of simulation time, with OPLS, KBFF, CHARMM, AMBER\*, and AMBER urea models, respectively.

times larger than that of water), which mainly derives from the stronger dispersion interaction of urea than water with nanotube (see Table S2 in Supporting Information). Consequently, each urea gains 2.55–4.58 kcal/mol on average as it penetrates the SWNT, whereas each water loses 0.12–1.64 kcal/mol on average for the same process. It should be noted that the replacement of structurally confined water molecules by larger urea molecules inside the nanotube core (on average each urea molecule can replace  $\sim 2.5$  water molecules<sup>35</sup>) is also favorable because of an overall solvent entropy gain. Thus, this interaction energy decomposition analysis shows the higher affinity of urea than water to the nanotubes as a result of stronger dispersion interaction of urea than water with hydrophobic nanotube.

To gain a deeper insight into the mechanism of this drying phenomenon, we have calculated the association free energy of a urea/water molecule with the carbon nanotubes by obtaining the potential of mean force (PMF) of a solvent molecule along the  $z$ -axis. The PMF of a solvent molecule  $i$ , denoted by  $W_i(z)$ , is calculated by integrating the mean force acting on the solvent

molecule  $i$  along the nanotube axis ( $z$ -axis);<sup>51</sup> i.e.,

$$W_i(z) - W_i(z_0) = \int_{z_0}^z \langle F_i(z') \rangle dz' \quad (2)$$

where  $z_0$  is the reference position (taken as 2.6 nm from the geometrical center of SWNT) where the PMF is set to zero. A total of four independent simulations (with the same system starting from different initial conditions) were run for force averaging, with data collected after the systems have reached equilibrium. Below, we only present the results using the OPLS urea model for illustration; the results for other urea models are similar. The total PMF of a urea and a water molecule along the  $z$ -axis are shown in Figure 2A. The association free energy (defined as the difference in the PMF for a solvent within SWNT vs bulk) is  $-0.89$  kcal/mol for a urea molecule, and  $+0.86$  kcal/mol for a water molecule, which indicates it is favorable for a urea molecule to move into the carbon nanotube while unfavorable for a water molecule to do so. The difference in the association free energy

**Table 4. Average Number of Urea ( $\langle N_{\text{urea}} \rangle$ ) and Water Molecules ( $\langle N_{\text{water}} \rangle$ ) in (6, 6) SWNT, as Well as the Drying Factors,  $f_{\text{drying}}$ , for Different Urea Models<sup>a</sup>**

Model	$\langle N_{\text{urea}} \rangle$	$\langle N_{\text{water}} \rangle$	$f_{\text{drying}}$
OPLS	2.701	0.333	35.1
KBFF	2.944	0.028	455
CHARMM	2.960	0.022	582
AMBER*	2.981	0.048	269
AMBER	2.962	0.005	2560

<sup>a</sup>These data were averaged over the last 90 ns.**Table 5. Differences in Average Interaction Energies (kcal/mol) for a Solvent Molecule in (6, 6) SWNT vs in Bulk, with Different Urea Models<sup>a</sup>**

model	$\Delta E_{\text{total}}^{\text{u}}$	$\Delta E_{\text{elec}}^{\text{u}}$	$\Delta E_{\text{vdW}}^{\text{u}}$	$\Delta E_{\text{total}}^{\text{w}}$	$\Delta E_{\text{elec}}^{\text{w}}$	$\Delta E_{\text{vdW}}^{\text{w}}$
OPLS	1.80	12.91	−11.11	2.83	7.01	−4.18
KBFF	−3.34	7.21	−10.55	3.10	7.17	−4.07
CHARMM	−2.94	7.77	−10.71	3.22	7.29	−4.07
AMBER*	−2.40	8.68	−11.08	1.91	5.62	−3.71
AMBER	−6.21	4.73	−10.94	4.41	9.03	−4.62

<sup>a</sup> $\Delta E_{\text{total}}^{\text{u}}$ ,  $\Delta E_{\text{elec}}^{\text{u}}$ , and  $\Delta E_{\text{vdW}}^{\text{u}}$  denote the differences in total, electrostatic, and vdW interaction energies, respectively, where ? is u for urea and w for water. These data were averaged over all of the 100 ns simulation time, because there are very few water molecules inside the SWNT.

between a urea and a water molecule is approximately 1.75 kcal/mol ( $\sim 2.9 k_{\text{B}}T$ ). To further understand the origin of these association free energies, the total PMFs of urea and water were decomposed into solvent–solvent and solvent–SWNT interaction components, as shown in Figure 2B. In the urea case, the gain in the solvent–SWNT free energy is larger than the loss in the solvent–solvent free energy; thus overall it is favorable, while, in the water case, the gain in the solvent–SWNT free energy is not large enough to offset the loss in the solvent–solvent free energy, thus unfavorable. These free energy decomposition analyses further confirm that the dominant driving force for the urea-induced drying is the stronger van der Waals interactions between urea and SWNT.

**3.2. Urea-Induced Drying for the (6, 6) SWNT System.** To investigate the influence of the diameters of nanotubes on the drying phenomenon, we also performed the simulation of the (6, 6) SWNT in 8 M aqueous urea (see Figure 3A). Parts B–F of Figure 3 show the number of urea and water molecules inside the cores of (6, 6) SWNTs as a function of simulation time, with five urea models. Remarkably, in all of the five cases, the (6, 6) SWNT is exclusively occupied by urea molecules. Even though water molecules occupy the (6, 6) SWNT initially, they can be expelled from the SWNT core within the first 4 ns. Table 4 lists the average number of solvent molecules and drying factors for the (6, 6) SWNT system with different urea models. These data were also averaged over the last 90 ns. We found that the urea-induced drying for the (6, 6) SWNT system was more remarkable compared to that for the (17, 8) SWNT system. As displayed in Table 4, the cases of OPLS and AMBER urea exhibit the weakest and the strongest drying effects, respectively, among the five cases, whereas the cases of KBFF, CHARMM, AMBER\* urea exhibit similar drying effects (the drying factors  $f_{\text{drying}}$  are in the same order of magnitude). Compared to the results of the (17, 8) SWNT system, the drying factors  $f_{\text{drying}}$  for the (6, 6) SWNT

system with all of the five urea models increased dramatically (the rank order also differs slightly). This is partly due to the steric effect, since each water molecule, though tiny, still has a finite size; after certain replacements by urea, there might be no room for a single water molecule, so the urea/water number ratio  $R_{\text{SWNT}}$  can be very large.

We also computed the interaction energies for a solvent molecule in the bulk region, and in (6, 6) SWNT, with the rest of the system (see Tables S3 and S4 in Supporting Information). Table 5 lists the differences in average interaction energies for a solvent molecule in (6, 6) SWNT vs in bulk, for all five urea models. Compared to the results of the (17, 8) system, both the loss in electrostatic interaction energies and the gain in vdW interaction energies increase, for a solvent moving from the bulk region to the SWNT core. Similar to the results of the (17, 8) system, the vdW interaction energy each urea gains is about 2–3 times larger than water gains, which mainly derives from the stronger dispersion interaction of urea than water with nanotube (see Table S4 in Supporting Information). Except for the case of OPLS urea, each urea gains 2.40–6.21 kcal/mol on average as it penetrates the SWNT, whereas each water loses 1.91–4.41 kcal/mol on average for the same process. In the case of OPLS urea, although each urea loses 1.80 kcal/mol on average as it penetrates the SWNT, each water loses more interaction energy (2.83 kcal/mol on average) for the same process. It should be noted that, although the solvent molecule which moves from the bulk region to the nanotube core loses interaction energy, it is still likely to penetrate the nanotube,<sup>41</sup> just like the case of the OPLS urea [it is very costly in overall free energy to leave a completely empty SWNT cavity, i.e., a dewetting transition; it is very rare to observe a dewetting transition since the water contact angle (and urea contact angle) with respect to the carbon nanotube has to be larger than 90°<sup>53,52</sup>]. These results suggest that the stronger dispersion interaction of urea than water with nanotube is the driving force for preferential occupancy of urea within (6, 6) SWNT too.

#### 4. CONCLUSIONS

In a previous report<sup>24</sup> we showed, when the carbon nanotubes were solvated in 8 M urea, urea molecules could induce the drying of hydrophobic nanotubes. In the present study, we further study this striking phenomenon with five different urea models to investigate if the drying phenomenon is sensitive to the urea models used. Interestingly, we have observed this urea-induced drying of nanotubes for all of the five models used in this study, despite that their nonbonded parameters, especially the charge distributions, are quite different. By decomposing the interaction energies for a urea and a water molecule into electrostatic and vdW components, we find that, in all of the five cases, the drying phenomenon results from the stronger dispersion interaction of urea than water with nanotube. Further, detailed calculations of the association free energy for solvent molecules with SWNT also indicate that the stronger dispersion interaction of urea than water with nanotubes is the predominant driving force for the urea-induced drying process. Although there are a few other urea models<sup>53–56</sup> reported in literature, we believe our current simulations with these five commonly used urea models are representative and adequate to demonstrate the robustness of the drying phenomenon as well as its underlying physical mechanism. Thus we conclude that the phenomenon of urea-induced drying of hydrophobic nanotubes and its physical



mechanism are qualitatively independent of the urea models. Consistent with our previous studies,<sup>19,24</sup> the present study implies the existence of a dry globule-like transient state during the urea-induced denaturation of proteins and supports the “direct interaction mechanism” whereby urea has a stronger dispersion interaction with protein than water. In addition, our study highlights the crucial role of dispersion interaction in the selective absorption<sup>31,32</sup> of molecules in hydrophobic nanopore, which may be important for nanoscience and nanotechnology.

## ■ ASSOCIATED CONTENT

**S Supporting Information.** Tables listing detailed data of interaction energies for a urea and a water molecule with the rest of the system and a complete citation for ref 25. This material is available free of charge via the Internet at <http://pubs.acs.org>.

## ■ AUTHOR INFORMATION

### Corresponding Author

\*E-mail: [ruhongz@us.ibm.com](mailto:ruhongz@us.ibm.com).

## ■ ACKNOWLEDGMENT

We thank Xiaowei Tang, Hangjun Lu, Xingling Tian, and Li Zeng for helpful discussions and comments. This work is partly supported by the National Natural Science Foundation of China (Grant Nos. 30870593 and 10825520), the China Postdoctoral Science Foundation (Grant No. 20090461385), and the Shanghai Supercomputer Center of China. P.D. and R.Z. acknowledge the support from the IBM BlueGene Program.

## ■ REFERENCES

- (1) Pace, C. N. *Methods Enzymol.* **1986**, *131*, 266.
- (2) Frank, H. S.; Franks, F. *J. Chem. Phys.* **1968**, *48*, 4746.
- (3) Wetlaufer, D. B.; Coffin, R. L.; Malik, S. K.; Stoller, L. *J. Am. Chem. Soc.* **1964**, *86*, 508.
- (4) Hammes, G. G.; Schimmel, P. R. *J. Am. Chem. Soc.* **1967**, *89*, 442.
- (5) Sagle, L. B.; Zhang, Y. J.; Litosh, V. A.; Chen, X.; Cho, Y.; Cremer, P. S. *J. Am. Chem. Soc.* **2009**, *131*, 9304.
- (6) Bennion, B. J.; Daggett, V. *Proc. Natl. Acad. Sci. U.S.A.* **2003**, *100*, S142.
- (7) Wei, H. Y.; Fan, Y. B.; Gao, Y. Q. *J. Phys. Chem. B* **2010**, *114*, 557.
- (8) Wei, H. Y.; Yang, L. J.; Gao, Y. Q. *J. Phys. Chem. B* **2010**, *114*, 11820.
- (9) Cafisch, A.; Karplus, M. *Structure* **1999**, *7*, 477.
- (10) Caballero-Herrera, A.; Nordstrand, K.; Berndt, K. D.; Nilsson, L. *Biophys. J.* **2005**, *89*, 842.
- (11) Robinson, D. R.; Jencks, W. P. *J. Am. Chem. Soc.* **1965**, *87*, 2462.
- (12) Auton, M.; Holthauzen, L. M. F.; Bolen, D. W. *Proc. Natl. Acad. Sci. U.S.A.* **2007**, *104*, 15317.
- (13) Lim, W. K.; Rosgen, J.; Englander, S. W. *Proc. Natl. Acad. Sci. U.S.A.* **2009**, *106*, 2595.
- (14) O'Brien, E. P.; Dima, R. I.; Brooks, B.; Thirumalai, D. *J. Am. Chem. Soc.* **2007**, *129*, 7346.
- (15) Klimov, D. K.; Straub, J. E.; Thirumalai, D. *Proc. Natl. Acad. Sci. U.S.A.* **2004**, *101*, 14760.
- (16) Stumpe, M. C.; Grubmuller, H. *PLoS Comput. Biol.* **2008**, *4*, No. e1000221.
- (17) Stumpe, M. C.; Grubmuller, H. *Biophys. J.* **2009**, *96*, 3744.
- (18) Canchi, D. R.; Paschek, D.; Garcia, A. E. *J. Am. Chem. Soc.* **2010**, *132*, 2338.
- (19) Hua, L.; Zhou, R. H.; Thirumalai, D.; Berne, B. J. *Proc. Natl. Acad. Sci. U.S.A.* **2008**, *105*, 16928.
- (20) Zangi, R.; Zhou, R. H.; Berne, B. J. *J. Am. Chem. Soc.* **2009**, *131*, 1535.
- (21) England, J. L.; Pande, V. S.; Haran, G. *J. Am. Chem. Soc.* **2008**, *130*, 11854.
- (22) Das, A.; Mukhopadhyay, C. *J. Phys. Chem. B* **2009**, *113*, 12816.
- (23) Yang, L.; Gao, Y. Q. *J. Am. Chem. Soc.* **2010**, *132*, 842.
- (24) Das, P.; Zhou, R. H. *J. Phys. Chem. B* **2010**, *114*, 5427.
- (25) MacKerell, A. D.; et al. *J. Phys. Chem. B* **1998**, *102*, 3586.
- (26) Duffy, E. M.; Severance, D. L.; Jorgensen, W. L. *Isr. J. Chem.* **1993**, *33*, 323.
- (27) Smith, L. J.; Berendsen, H. J. C.; van Gunsteren, W. F. *J. Phys. Chem. B* **2004**, *108*, 1065.
- (28) Weerasinghe, S.; Smith, P. E. *J. Phys. Chem. B* **2003**, *107*, 3891.
- (29) Sorin, E.; Pande, V. *Biophys. J.* **2005**, *88*, 2472.
- (30) Zhou, R.; Huang, X.; Margulis, C. J.; Berne, B. J. *Science* **2004**, *305*, 1605.
- (31) Liu, Y.; Consta, S.; Goddard, W. A. *J. Nanosci. Nanotechnol.* **2010**, *10*, 3834.
- (32) Lee, J.; Aluru, N. R. *Appl. Phys. Lett.* **2010**, *96*, 133108.
- (33) Stumpe, M. C.; Grubmuller, H. *J. Phys. Chem. B* **2007**, *111*, 6220.
- (34) Kokubo, H.; Rosgen, J.; Bolen, D. W.; Pettitt, B. M. *Biophys. J.* **2007**, *93*, 3392.
- (35) Kokubo, H.; Pettitt, B. M. *J. Phys. Chem. B* **2007**, *111*, 5233.
- (36) Kang, M.; Smith, P. E. *Fluid Phase Equilib.* **2007**, *256*, 14.
- (37) Lee, M. E.; van der Vegt, N. F. A. *J. Am. Chem. Soc.* **2006**, *128*, 4948.
- (38) Zhou, R.; Eleftheriou, M.; Royyuru, A. K.; Berne, B. J. *Proc. Natl. Acad. Sci. U.S.A.* **2007**, *104*, 5824.
- (39) Jorgensen, W. L.; Chandrasekhar, J.; Madura, J. D.; Impey, R. W.; Klein, M. L. *J. Chem. Phys.* **1983**, *79*, 926.
- (40) Humphrey, W.; Dalke, A.; Schulten, K. *J. Mol. Graphics* **1996**, *14*, 33.
- (41) Hummer, G.; Rasaiah, J. C.; Noworyta, J. P. *Nature* **2001**, *414*, 188.
- (42) Xiu, P.; Zhou, B.; Qi, W. P.; Lu, H. J.; Tu, Y. S.; Fang, H. P. *J. Am. Chem. Soc.* **2009**, *131*, 2840.
- (43) Hess, B.; Kutzner, C.; van der Spoel, D.; Lindahl, E. *J. Chem. Theory Comput.* **2008**, *4*, 435.
- (44) Bussi, G.; Donadio, D.; Parrinello, M. *J. Chem. Phys.* **2007**, *126*, 014101.
- (45) Parrinello, M.; Rahman, A. *J. Appl. Phys.* **1981**, *52*, 7182.
- (46) Darden, T.; York, D.; Pedersen, L. *J. Chem. Phys.* **1993**, *98*, 10089.
- (47) Brown, R. D.; Godfrey, P. D.; Storey, J. J. *Mol. Spectrosc.* **1975**, *58*, 445.
- (48) Kumler, W. D.; Fohlen, G. M. *J. Am. Chem. Soc.* **1942**, *64*, 1944.
- (49) Gilkerson, W. R.; Srivastava, K. K. *J. Phys. Chem.* **1960**, *64*, 1485.
- (50) Lefebvre, J. *Solid State Commun.* **1973**, *13*, 1873.
- (51) Kjellander, R.; Greberg, H. *J. Electroanal. Chem.* **1998**, *450*, 233.
- (52) Li, X.; Li, J. Y.; Eleftheriou, M.; Zhou, R. H. *J. Am. Chem. Soc.* **2006**, *128*, 12439.
- (53) Tsai, J.; Gerstein, M.; Levitt, M. *J. Chem. Phys.* **1996**, *104*, 9417.
- (54) Zou, Q.; Bennion, B. J.; Daggett, V.; Murphy, K. P. *J. Am. Chem. Soc.* **2002**, *124*, 1192.
- (55) Caballero-Herrera, A.; Nilsson, L. *J. Mol. Struct. (THEOCHEM)* **2006**, *758*, 139.
- (56) Sokolic, F.; Idrissi, A.; Perera, A. *J. Chem. Phys.* **2002**, *116*, 1636.